Volume 2 | Number 32 | 28 August 2014 | Pages 12603–13170

Journal of Materials Chemistry A

Materials for energy and sustainability

www.rsc.org/MaterialsA

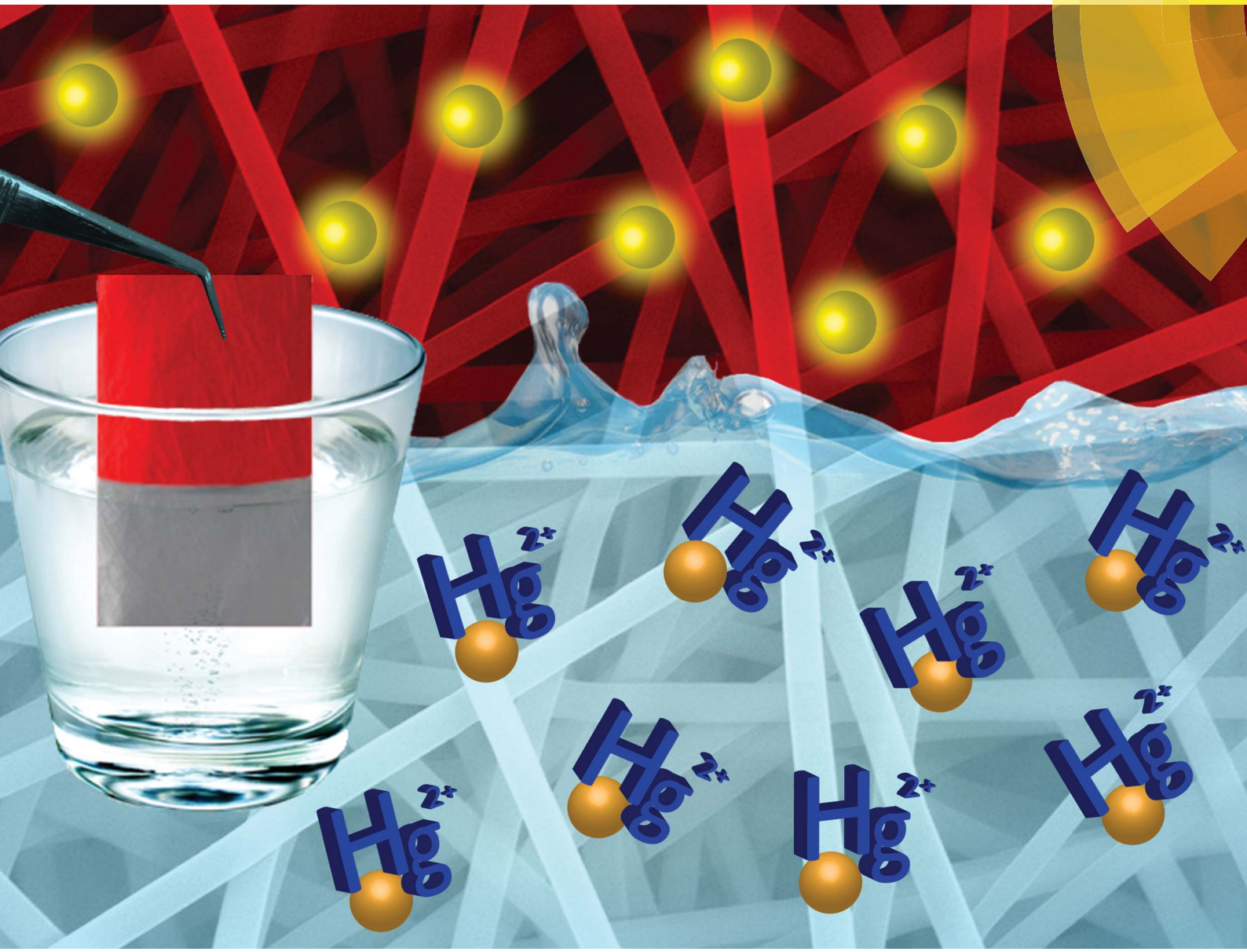

ISSN 2050-7488

ROYAL SOCIETY OF CHEMISTRY

PAPER

Anitha Senthamizhan, Tamer Uyar *et al.*

Flexible and highly stable electrospun nanofibrous membrane incorporating gold nanoclusters as an efficient probe for visual colorimetric detection of Hg(II)

Journal of Materials Chemistry A

PAPER

View Article Online
View Journal | View Issue

Cite this: J. Mater. Chem. A, 2014, 2, 12717

Flexible and highly stable electrospun nanofibrous membrane incorporating gold nanoclusters as an efficient probe for visual colorimetric detection of Hg(II)†

Anitha Senthamizhan,*[a] Asli Celebioglu[ab] and Tamer Uyar*[ab]

Here, we describe the visual colorimetric detection of Hg^{2+} based on a flexible fluorescent electrospun nanofibrous membrane (NFM). It is an efficient approach, in which we have effectively integrated fluorescent gold nanoclusters (AuNC) into electrospun polyvinyl alcohol nanofibers. Interestingly, the resulting composite nanofibers (AuNC*NFM) are shown to retain the fluorescence properties of AuNC and exhibit red fluorescence under UV light, being cogent criteria for the production of a visual colorimetric sensor. Furthermore, capabilities with regard to the stability of the AuNC*NFM have been under observation for a period of six months, with conditions matching those of typical atmosphere, and the resulting outcome has thrown light on their long-term storability and usability. It is clear, from the fact that the nanofibrous membrane preserves the fluorescence ability up to a temperature of 100 °C, that temperature does not have an effect on the sensing performance in real-time application. The water-insoluble AuNC*NFM have been successfully tailored by cross-linking with glutaraldehyde vapor. Further, the contact mode approach has been taken into consideration for the visual fluorescent response to Hg^{2+}, and the observed change of color indicates the utility of the composite nanofibers for onsite detection of Hg^{2+} with a detection limit of 1 ppb. The selectivity of the AuNC*NFM hybrid system has been analyzed by its response to other common toxic metal interferences (Pb^{2+}, Mn^{2+}, Cu^{2+}, Ni^{2+}, Zn^{2+}, Cd^{2+}) in water. Several unique features of the hybrid system have been determined, including high stability, self-standing ability, naked-eye detection, selectivity, reproducibility and easy handling – setting a new trend in membrane-based sensor systems.

Received 7th May 2014
Accepted 27th May 2014

DOI: 10.1039/c4ta02295e

www.rsc.org/MaterialsA

Introduction

Water serves as an essential and vital need for the wellbeing and sustenance of life. In some cases, however, the water quality becomes compromised by the presence of infectious agents and toxic metals.[1] This effect – primarily caused by industrial, agricultural and household factors – eventually causes damage to the environment and human health. Among the many causes of water pollution, those generated by the use of heavy-metal ions pose a serious threat to mankind and have been a topic of concern for decades now. Most importantly, mercury stands out as a prime example of a heavy metal causing damage to the nervous system even when present in parts per million (ppm) concentration. After extensive research and exploration, while the European Union has determined 1 ppb as being a tolerable limit for mercury in drinking water, United States Environmental Protection Agency (US EPA) has set national regulations for the maximum contaminant level of mercury in drinking water to be 2 ppb, that has no adverse health effects.[2]

The presence of Hg^{2+} causes various environmental and health problems evoking high interest and speculation and further in-depth research for identifying and eradicating this toxic component in water. Over the past few decades, various techniques have been devised for monitoring mercury levels using atomic absorption spectroscopy, electrochemical sensors, chromatography and several other techniques.[3–9] But most of them have certain disadvantages, such as multistep sample preparation, and also have proved to be expensive. Amongst all these techniques, colorimetric assay of Hg^{2+} has gained a lot of attention among scientists owing to its convenience, facile monitoring, and no requirement of sophisticated instruments.[10–12] The application of noble metal nanoparticles for water purification and their contribution in detecting toxic metals dates back a long time. Besides, recent effort on fluorescent gold nanoclusters has made them a new platform for developing mercury sensors owing to their promising

[a]UNAM-National Nanotechnology Research Centre, Bilkent University, Ankara, 06800, Turkey. E-mail: senthamizhan@unam.bilkent.edu.tr; uyar@unam.bilkent.edu.tr
[b]Institute of Materials Science & Nanotechnology, Bilkent University, Ankara, 06800, Turkey

† Electronic supplementary information (ESI) available. See DOI: 10.1039/c4ta02295e

characteristics of operational simplicity, cost-effectiveness, easy visualization and high sensitivity.[13–18] However, the reported techniques, being mostly solution-based, have resulted in stability problems, limiting their potential effectiveness and practical applications. Moreover, a sensing mediator is required to be mixed with the analyte medium, and the corresponding responses are monitored *in situ* with respect to optical responses, making the sensor inefficient. This leads to a need to develop a novel and modern method to fabricate a solid template-based sensor on a large scale for technological applications.[19–22]

To make this possible for day-to-day usage, luminescent metal clusters are designed and integrated into a solid matrix which provides an easy platform to maintain their stability and easy accessibility for probe analytes. However, due to the solid support having a low specific surface area, it affects the reactivity and sensitivity of the sensor performance.[23–30] The features of a high surface area and good flexibility are supposed to overcome these disadvantages. When comparing various techniques, electrospinning provides versatility for the fabrication of functional nanofibers and incorporation of active agents into the nanofiber matrix.[31,32] Essentially, electrospun nanofibrous membranes are flexible, cost-effective, relatively easy to handle and have accurate reproducibility.

Herein, we present an effective synthesis to produce highly luminescent gold nanoclusters (AuNC) embedded in an electrospun polyvinyl alcohol (PVA) nanofibrous membrane (NFM), termed AuNC*NFM, for efficient detection of Hg^{2+}. However, fabricating a flexible polymeric NFM composed of AuNC for sensing applications raises several issues that need to be addressed, regarding aggregation, fluorescence quenching in the nanofibers, and stability over time and temperature. In order meet these requirements, a suitable polymer matrix that does not quench the luminescence intensity of the AuNC has to be chosen. Another important consideration is the problem of incorporation of the aqueous AuNC into a hydrophobic polymer matrix due to their incompatibility. Consequently, PVA is chosen as a support matrix due to its nontoxicity, electrospinnability, and compatibility. All the same, the obtained nanofibrous composite mat is rapidly dissolved in water, further limiting its applications. Thus, a water-insoluble PVA nanofibrous mat was prepared by cross-linking with glutaraldehyde (GA) vapor for an optimal period of time and at a suitable concentration.

Experimental

Materials and methods

Tetrachloroauric acid trihydrate ($HAuCl_4 \cdot 3H_2O$, Sigma-Aldrich), bovine serum albumin (BSA, Sigma-Aldrich), PVA (Scientific Polymer, 88% hydrolyzed, M_w 125 000), mercuric acetate (Merck), zinc acetate dihydrate (Sigma-Aldrich, ≥98%), lead(II) nitrate (Sigma-Aldrich, ≥99.0%) copper(II) acetate hydrate (Sigma-Aldrich, 98%), cadmium nitrate tetrahydrate (Fluka) and cobalt(II) acetate tetrahydrate (SIAL) were purchased. Deionized water was used from a Millipore Milli-Q Ultrapure Water System. Stock solutions of metal ions (50 ppm) prepared in deionized water and a further standard solution used for calibration were prepared by gradually diluting the stock solution in water with a concentration range from 50 ppm to 10 ppt.

Preparation of fluorescent gold nanoclusters (AuNC)

The fluorescent gold nanoclusters were prepared according to a previously reported method.[33] According to this method, approximately 10 mM of $HAuCl_4$ solution (10 ml) was added to an equal amount of BSA solution (50 mg ml^{-1}) at 37 °C with vigorous stirring. Two minutes later, 1 ml of 1 M NaOH solution was introduced into the mixture, and the reaction was allowed to proceed accompanied by vigorous stirring at 37 °C for a time period of 12 hours. The thus prepared AuNC emitted red fluorescence under exposure to UV light. They were then subject to a further process to incorporate them into the nanofibers.

Electrospinning of PVA nanofibers and gold nanocluster-incorporated PVA nanofibers

The precursor PVA solution used for electrospinning was prepared by dissolving PVA (7.5 wt%) granules in deionized water at 80 °C by gentle magnetic stirring for 6 hours. After the solution was brought to room temperature, various concentrations of gold cluster solution were added to the PVA solution. The processing parameters, including viscosity (7.5 wt%), flow rate (0.5), applied voltage (10 kV) and distance between the electrodes (10 cm), were subjected to optimization and further processed, leading to defect-free PVA nanofibers and AuNC*NFs. The electrospinning process was carried out at room temperature in a closed Plexiglass box. A protracted collection time of 2–4 hours was used to give a self-standing flexible fibrous membrane.

Cross-linking of electrospun PVA and AuNC*NF mat

The cross-linking of PVA and AuNC*NF was carried out with glutaraldehyde (GA) vapor. Accordingly, the GA solution was mixed with HCl (32% w/v, as catalyst) in the volume ratio of 3 : 1 (GA–HCl). The resultant solution was spread out into a Petri dish and placed at the bottom of a desiccator (20 cm in diameter and 20 cm in height). Then, PVA–NFM and AuNC*NFM were positioned into the sealed desiccator by using a metal wire without physical contact and exposed to a GA vapor atmosphere for 24 h. Subsequently, they were taken out of the desiccator and kept in a vacuum oven to remove the unreacted vapor molecules adsorbed by the samples.

Contact-mode visual detection of Hg^{2+}

As the next step in the process, the flexible nanofibrous membrane was cut uniformly into small pieces of size 2 cm × 3 cm and then dipped in different concentrations of Hg^{2+} separately for 10 minutes. Subsequent to solvent evaporation, the membrane was illuminated with UV light to study and confirm the color changes. All the procedures were repeated and analyzed in order to ensure consistency in analyzing the membrane. A similar procedure was also carried out for

different metal ions in water (Pb^{2+}, Cu^{2+}, Zn^{2+}, *etc.*). For confocal laser scanning microscopy (CLSM), the nanofibers were coated on separate glass slides and dipped in Hg^{2+} solution for 2 minutes. After drying the solvent, images were taken at a magnification of ×20.

Instrumentation

Using scanning electron microscopy (SEM), the morphology of the nanofibers was observed and their diameter measured (Quanta 200 FEG). The presence of elements in the AuNC*NF was analyzed by the application of transmission electron microscopy (TEM, Tecnai G2 F30). Fluorescence emission spectra were measured using a time-resolved fluorescence spectrophotometer (FL-1057 TCSPC). CLSM images were recorded using a Zeiss LSM 510, wherein excitation sources were fixed at 488 nm for all experiments and the images were captured at ×20 magnification.

Results and discussion

The design of the sensor strip was optimized on the basis of five decisive criteria here: (1) fine homogeneity of AuNC in the nanofibers, (2) stability against time and temperature, (3) insoluble nature in water, (4) specific response to Hg^{2+} and (5) significant visual colorimetric detection. Collectively, the effort produced optimistic results. The SEM images of randomly oriented electrospun PVA nanofibers and AuNC*NFs show a defect-free morphology with a relatively uniform diameter of 180 ± 40 nm, as depicted in Fig. 1a and b.

Also, careful observation reveals the fact that the surface is rough compared with bare PVA nanofibers, highlighting the partial exposure of the gold nanoclusters on the surface. Additionally, scanning transmission electron microscopy (STEM) elemental mapping of an AuNC-embedded single PVA nanofiber confirms that the spatial distribution of AuNC along the nanofiber is uniform, as illustrated in Fig. 1c. This uniform allocation and configuration significantly enhances the purity and homogeneity of the color, which is of paramount importance for the colorimetric sensing properties. Furthermore, on exposure to UV light (366 nm), the AuNC*NFM emit a bright red fluorescence which is the characteristic emission of gold nanoclusters, as shown in Fig. 2a and b. Confirmed by the results, this approach is important for retaining the original fluorescence efficiency of the AuNC (see Fig. S1, ESI†) in the PVA nanofibrous matrix, which is further established from the CLSM images (Fig. 2c and d). The observed fluorescence is uniform throughout the nanofibers, suggesting the homogeneous distribution of gold nanoclusters in the nanofibers. The uniformity and homogeneity of the nanofibers are mostly distorted by the varied concentration of the gold nanoclusters that are to be loaded. Initially, the effect of concentration of the AuNC in the polymer solution on the morphology of the electrospun nanofibers was characterized using SEM, as shown in Fig. S2, ESI.† However, no distinct dissimilarity is seen with regard to the diameter or the structure of the nanofibers. Moreover, variations in the proportion of AuNC in the composite nanofibers show minute color discrepancies ranging from a light red to a dark red color with respect to their increased concentrations (see Fig. 3a–e). Thus, the structural features and functional properties of the nanofibrous membranes can be effectively adjusted by tailoring the concentration of their AuNC constituents.

Fig. 3 depicts the fluorescence spectra of AuNC*NFM with different concentrations of AuNC. As noticed in the spectra, the

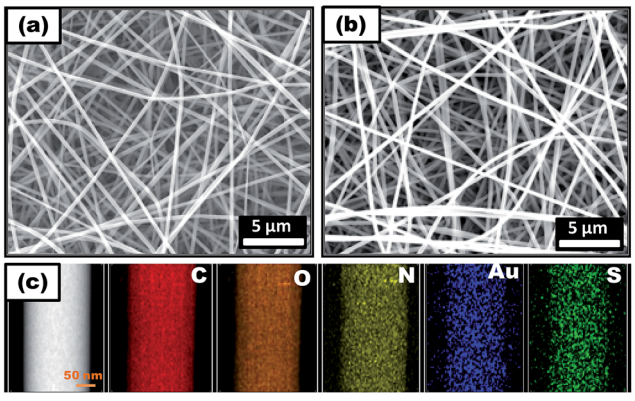

Fig. 1 SEM images of the PVA nanofibers (a) and gold nanocluster (4 wt%)-embedded PVA nanofibers (b). (c) HAADF-STEM (high-angle annular dark-field scanning transmission electron microscopy) image and mapping of the elements C, O, N, S and Au present in the AuNC*NF.

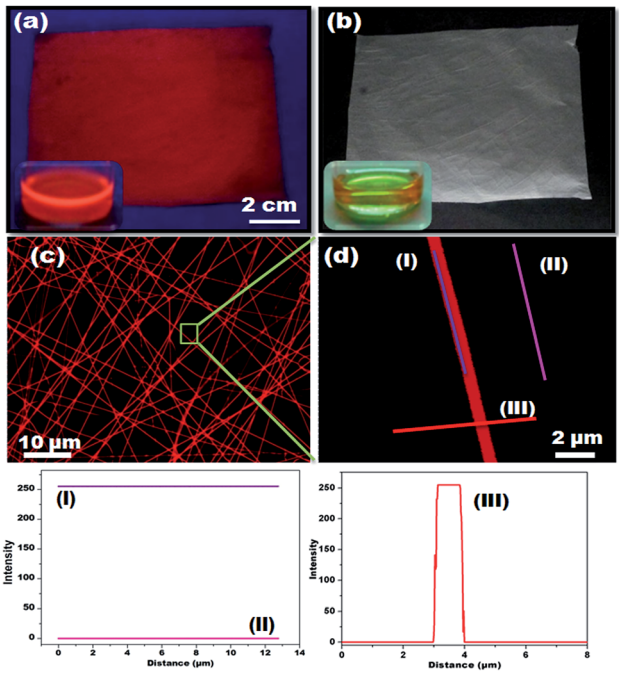

Fig. 2 Photographs of the AuNC*NFM under (a) UV light (λ_{ext} = 366 nm) and (b) white light. Insets show photographs of AuNC solution taken under the same conditions. (c) CLSM image of the AuNC*NF excited at 488 nm. (d) Isolated single AuNC*NF and intensity data collected from the surface. The intensity reached maximum (I) on the NF surface and it was zero (II) where there was no NF. Further, measurement was carried out across the NF(III).

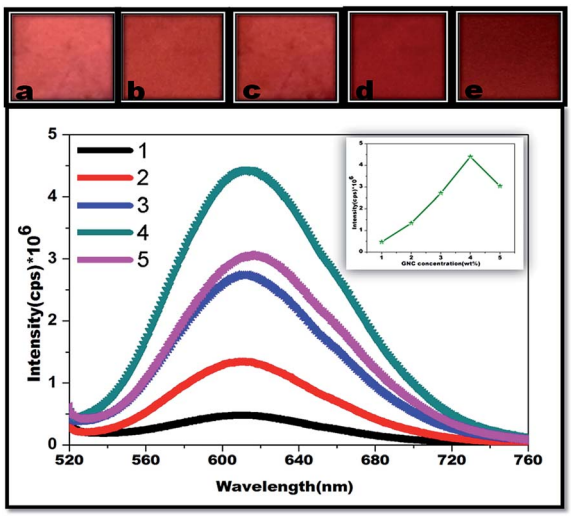

Fig. 3 Fluorescence spectra of AuNC*NFM with different concentrations of gold nanoclusters (1, 1 wt%; 2, 2 wt%; 3, 3 wt%; 4, 4 wt%; 5, 5 wt%) and corresponding photographs taken under UV light (a–e).

intensity of the emission increases to about 4 wt% of AuNC, followed by a gradual decrease; and there is a shift towards longer wavelengths, accompanied by a broadening of the peak.

Analyzing the observations, this could be due to the increase in the concentration of AuNC, ultimately leading to a decrease in the inter-particle distance in the nanofibrous film. Subsequently, this also shows a superlative result for the coupling effect between the nanoparticles, leading to aggregation at higher concentrations.[34–36] However, the enlarged surface area, known for its rapid evaporation rate, leads to a decreased aggregation, because of which immediate solidification retards the further growth of the clusters inside the matrix.[37–40]

Secondly, the AuNC have a tendency to be sensitive to various factors, including the nature of the ligands, size, environment and temperature.[41,42] A comparison of photoluminescence spectra of AuNC solution and AuNC*NFM is shown in Fig. 4. It is evident that the deconvoluted spectra confirm the presence of

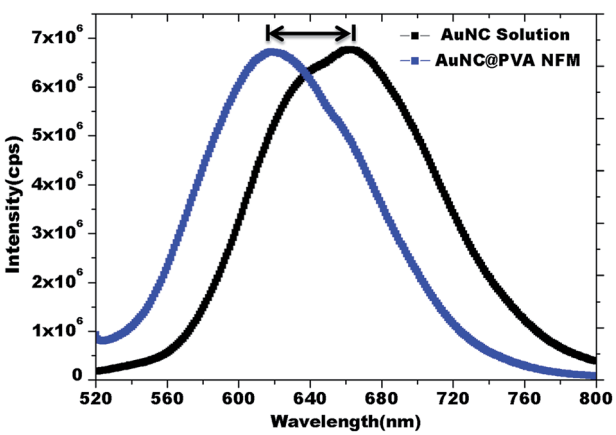

Fig. 4 Comparison of emission spectra of AuNC solution and AuNC*NFM (λ_{ext} = 500 nm).

two bands, originating from the stable Au core (Band I) and Au–S (Band II) as illustrated in Fig. S3, ESI.†[43] There is also a remarkable phenomenon observed at this juncture in that the fluorescence emission of AuNC*NFM shows a blue shift with a decreased bandwidth, when compared with the results for the solution state. With further study of the results, it is noticed that these happenings might arise for two reasons: (1) the strong confinement and well-organized nature of the cluster assembly in the nanofibrous matrix; and (2) the polarity of the local environment of the gold nanoclusters – *i.e.*, the local dielectric environment of AuNC in the nanofibers is less polar than that of AuNC dispersed in solution.[44,45]

We subsequently evaluated the fluorescence stabilities of AuNC*NF since the AuNC emissions in solution state decreased with time when exposed to typical atmosphere at room temperature, and this is detrimental to the development of practical applications for these sensors. In the present case, the nanofibrous membrane was left at room temperature for a prolonged period of time, say 1 to 6 months, and then CLSM images were recorded (see Fig. S4, ESI†). The observed results confirm that there is no significant decrease in the emission intensity and the AuNC*NFM continues to maintain red fluorescence under UV light. It is suggested that the wrapping of polymer chains around the fluorescent nanoclusters provides a protective environment, thereby improving AuNC stability. Thus the electrospun nanofibers not only enhance the stability of the system, but also retain its characteristic emission features, stressing the extended storability and usability.

To elucidate the thermal stability of the AuNC*NFM, the membrane was treated at different temperatures from 50 °C to 175 °C. Fig. S5, ESI† shows the luminescence profiles with photographs of the AuNC*NFM treated at different temperatures. As expected, the intensity is seen to be increased at 50 °C resulting from the removal of water molecules adsorbed on the surface. The fluorescence feature of AuNC*NFM is well maintained at around 100 °C, which implies that the membranes are durable against heat – a useful attribute for outdoor sensor applications. In continuing the process, though, thermal annealing beyond 100 °C drastically decreases the emission intensity of the sensor.

The undetermined blue-shifts result from the reduced stability of the surface in nanoclusters which are known to be caused by the degradation of BSA. We have thus obtained a distinct fluorescence emission change and the subsequent nanofiber structure has finally not been changed as illustrated in Fig. S6, ESI.† The obtained nanofibrous mat was found to be rapidly soluble in water. Hence, the AuNC*NFM is further cross-linked with glutaraldehyde vapor.[46–48] As observed in Fig. 5, the morphology (Fig. 5a) and the fluorescent nature (Fig. 5b) of the nanofibers remain unchanged after cross-linking. It is suggested that the spatial distribution of the AuNC is kept unchanged which was further confirmed by HAADF-STEM mapping (Fig. S7†). Its stability has been tested by immersing the membrane in water for 24 hours and the unaffected morphology proves its durability (see Fig. S8, ESI†). The flexible nature of the cross-linked NFM does not alter even though the

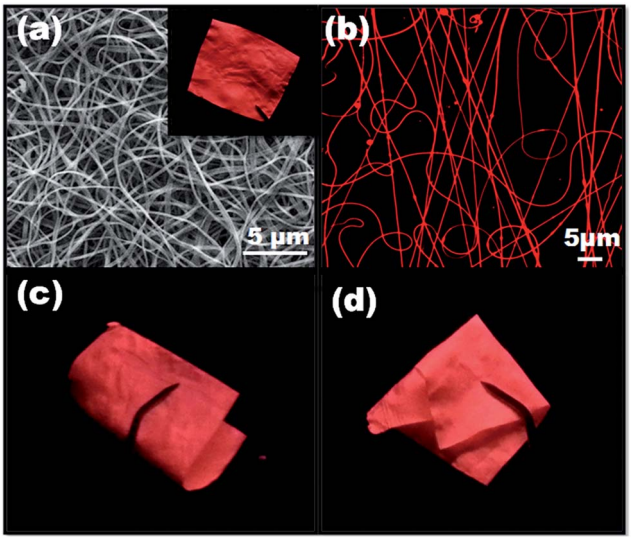

Fig. 5 (a) SEM image of the cross-linked AuNC*NFM. Inset shows a photograph taken under UV light. (b) CLSM image of the AuNC*NF. (c and d) Flexible nature of the nanofibrous membrane.

membrane becomes relatively hard compared with as-spun NFM, which is clearly observed in Fig. 5c and d.

As known parameters in sensor performance, the metal ion selectivity and binding kinetics are strongly dependent on the morphology of the sensor system, acting as a leading force towards the phenomenon of fluorescence quenching. Also, partially dispersed gold nanoclusters in the electrospun nanofibers are expected to quench the fluorescence more efficiently than the interfacially segregated AuNC in the solution-cast film. Besides, an electrospun nanofiber enables the expedient diffusion of analyte molecules into the nanofibrous matrix, accelerating the sensitive response of Hg^{2+} sensing.[49,50] The sensing performance of AuNC*NFM towards mercury ions in an aqueous solution has been tested in diverse approaches using (a) fluorescence spectra and (b) visual colorimetric response through contact-mode and CLSM-based analysis. Equilibrium fluorescence quenching has been reached within 10 minutes, which might result from the rapid interaction between the analytes and gold nanoclusters (see Fig. S9†). Therefore, the AuNC*NFM strip was immersed in the Hg^{2+} solution for 10 minutes and then taken out from the solution for further studies. The variation in the emission features of AuNC*NFM have been investigated upon exposure to different concentrations of Hg^{2+}, using fluorescence spectra as depicted in Fig. S10, ESI.† Apparently, the fluorescence intensity is shown to decrease with increasing concentrations of Hg^{2+}, due to the strong metallophilic bond established between Hg^{2+} and Au^{+}.[51–53] Notably, the detection limit is concluded to be a valuable limit of 0.1 ppb according to the US EPA, which has defined a maximum permitted level of mercury in drinking water as 2 ppb. The morphology of the AuNC*NFM is not affected after addition of Hg^{2+}, as shown in Fig. S11, ESI.†

Further, an analysis of the visual colorimetric response of the sensor strips toward various concentrations of Hg^{2+} was carried out. First, the membrane strip was immersed in water in the absence of Hg^{2+}. This resulted in insignificant changes in the fluorescence behavior when viewed by the naked eye. For ease of visualization, half of each piece of the membrane strip was dipped into the mercury solution and the other half was maintained as a reference, as clearly depicted in Fig. 6. It is of interest that the sensor displayed distinguishable color changes from red to dark blue with increasing Hg^{2+} concentration, detectable with the naked eye up to 50 ppb. However, even though there has been a decrease in the red color with a decrease in concentration, changes are not visible below the described concentration.

The mechanism for changes of color upon exposure to Hg^{2+} can be understood as follows. The higher surface area of the nanofibers facilitates more adsorption of Hg^{2+} ions on their surface, resulting in rapid desorption of capping molecules from the AuNC surface, which in turn leads to changes of color from red to blue. The observed changes in color could not be retained even after prolonged time, indicating that there could be adsorption of Hg^{2+} on the surface of the AuNC. Additionally, sensor strips fabricated from different batches exhibited identical sensing responses, which implies a consistency of the performance.

Typically, the incubation time is long (~10 to 30 minutes) to observe the visual response of the sensor. For further exploration of the function of the detection system for Hg^{2+}, the sensing performance of mercury was investigated by the CLSM method, as depicted in Fig. 7. Conspicuously, the visual detection limit is extended up to 1 ppb and differences in the fluorescence intensity are monitored within a time frame of 2 minutes. The competing chemical interferences of the toxic metal ions in water pose a problem with the conventional detection approach for selective determination of mercury. Subsequently, selectivity has been investigated by testing the

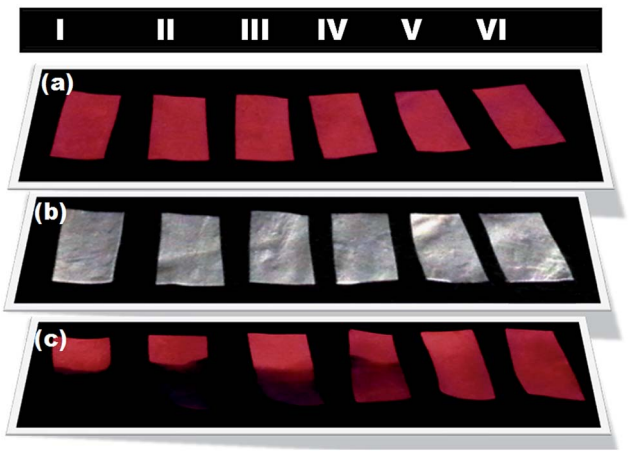

Fig. 6 Visual colorimetric detection of Hg^{2+} by the contact-mode approach. Photographs of the AuNC*NFM strip before Hg^{2+} treatment viewed under UV (a) and white (b) light. Fluorescence quenching of AuNC*NFM strips (c) by different concentrations of Hg^{2+} when viewed under UV light ((I) 1 ppm; (II) 100 ppb; (III) 50 ppb; (IV) 20 ppb; (V) 10 ppb; (VI) 1 ppb). Half of each piece of the membrane strip is dipped in the Hg^{2+} solution and the other half is maintained as a reference for a clear visualization of color change.

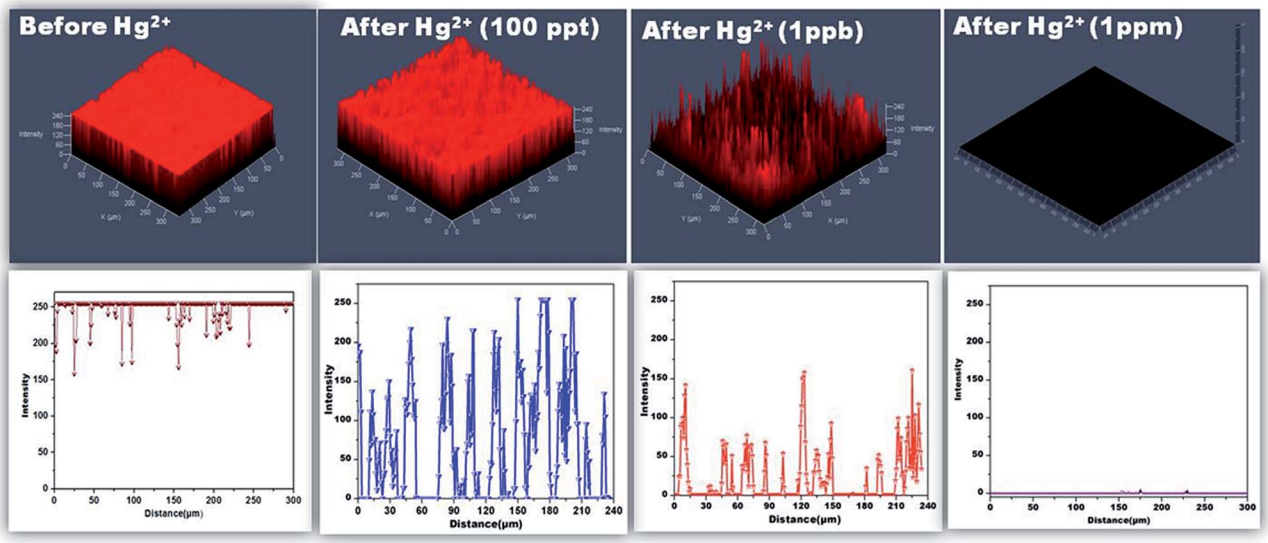

Fig. 7 CLSM images of the AuNC*NFs before and after treatment of Hg^{2+} and their intensity data collected across the nanofibrous membrane surface (λ_{ext} = 488 nm, ×20 magnification).

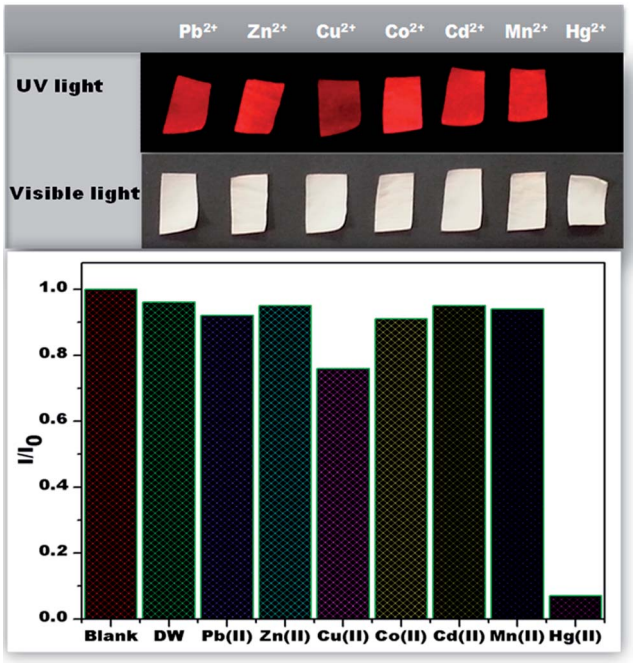

Fig. 8 Sensing performance of AuNC*NFM upon exposure to different metal ions in water. The concentration of all metal ions was fixed at 10 ppm. Photographs were taken under UV and white light.

response of the sensor towards Pb^{2+}, Cd^{2+}, Mg^{2+}, Cu^{2+}, Zn^{2+} and Co^{2+} at higher concentrations (say 10 ppm), and the corresponding visual fluorescence response is illustrated in Fig. 8.

It is interesting to note that, except for Hg^{2+}, no obvious deviations are observed, whereas in contrast it was found that the Cu^{2+} ions revealed a slight decrease in their fluorescence intensity. However, as the concentration goes down, there was no more quenching for Cu^{2+} ions, and additionally luminescence was completely quenched for Hg^{2+}. Furthermore, no color change is observed for the other ions except Hg^{2+}, with its original color being retained. This exclusive and unique color change of the Hg^{2+}-treated membrane strip substantiates the fact that the selective detection could also be visualized with the naked eye.

Conclusions

To conclude, highly fluorescent and flexible AuNC*NFM have been produced by an efficient method of electrospinning, exhibiting solid stability and steadiness over extended periods of time in an applicable environment involving temperatures up to 100 °C. A successful procedure has been described for the preparation of a water-stable membrane by cross-linking the resultant membrane with glutaraldehyde vapor. Evidently, this is the first-ever example showcasing the incorporation of fluorescent gold clusters in electrospun nanofibers for the efficient detection of Hg^{2+} in aqueous solutions. The resultant color change coupled with the selective coordination of Hg^{2+} has successfully demonstrated trouble-free "naked eye" colorimetric sensing. The very useful features of high stability, sensitivity and selectivity have emphasized the utility of the sensor, indicating its practical applications in the environmental monitoring of toxic mercury. However, more in-depth research needs to be encouraged to improve the sensitivity of the system towards visual colorimetric detection. Inspiringly, other studies have been initiated to explore more on the discussed topic.

Acknowledgements

A.S. thanks the Scientific & Technological Research Council of Turkey (TUBITAK) (TUBITAK-BIDEB 2216, Research Fellowship

Programme for Foreign Citizens) for a postdoctoral fellowship. A.C. acknowledges TUBITAK-BIDEB for the national PhD study scholarship. T.U. acknowledges partial support of EU FP7-Marie Curie-IRG for funding NANOWEB (PIRG06-GA-2009-256428) and The Turkish Academy of Sciences – Outstanding Young Scientists Award Program (TUBA-GEBIP). The authors thank M. Guler for TEM-STEM analysis.

Notes and references

1 EPA, U.S., Drinking Water Contaminants, http://water.epa.gov/drink/contaminants/index.cfm#List, accessed on 31 12 11.
2 (*a*) European Union, OJ L 330/42 5.12.98, 1998; (*b*) EPA (US Environmental Protection Agency) established the mercury(II) limit as 2 ppb, 2006, EPA-HQ-OPPT-2005-0013.
3 Z. Zhu, Y. Su, J. Li, D. Li, J. Zhang, S. Song, Y. Zhao, G. Li and C. Fan, *Anal. Chem.*, 2009, **81**, 7660.
4 W. R. Hatch and W. L. Ott, *Anal. Chem.*, 1968, **40**, 2085.
5 J. H. An, S. J. Park, O. S. Kwon, J. Bae and J. Jang, *ACS Nano*, 2013, **7**, 1056.
6 T. Balaji, A. Sherif, E. Safty, H. Matsunaga, T. Hanaoka and F. Mizukami, *Angew. Chem., Int. Ed.*, 2006, **45**, 7202.
7 Q. Wei, R. Nagi, K. Sadeghi, S. Feng, E. Yan, S. J. Ki, R. Caire, D. Tseng and A. Ozcan, *ACS Nano*, 2014, **8**, 1121.
8 W. Ren, C. Zhu and E. Wang, *Nanoscale*, 2012, **4**, 5902.
9 G. L. Wang, J. J. Xu and H. Y. Chen, *Nanoscale*, 2010, **2**, 1112.
10 H. N. Kim, W. X. Ren, J. S. Kim and J. Yoon, *Chem. Soc. Rev.*, 2012, **41**, 3210.
11 P. Wu, T. Zhao, S. Wang and X. Ho, *Nanoscale*, 2014, **6**, 43.
12 J. Zhang and S. H. Yu, *Nanoscale*, 2014, **8**, 4096.
13 G. S. Anand, A. I. Gopalan, S.-W. Kang and K.-P. Lee, *J. Anal. At. Spectrom.*, 2013, **28**, 488.
14 J. Liu, X. Ren, X. Meng, Z. Fang and F. Tang, *Nanoscale*, 2013, **5**, 10022.
15 D. Lu, C. Zhang, L. Fan, H. Wu, S. Shuang and C. Dong, *Anal. Methods*, 2013, **5**, 5522.
16 X. Yuan, T. J. Yeow, Q. Zhang, J. Y. Lee and J. Xie, *Nanoscale*, 2012, **4**, 1968.
17 X. Yuan, Z. Luo, Y. Yu, Q. Yao and J. Xie, *Chem.–Asian J.*, 2013, **8**, 858.
18 S. Chen, D. Liu, Z. Wang, X. Sun, D. Cui and X. Chen, *Nanoscale*, 2013, **5**, 6731.
19 Y. Si, X. Wang, Y. Li, K. Chen, J. Wang, J. Yu, H. Wang and B. Ding, *J. Mater. Chem. A*, 2014, **2**, 645.
20 Y. Zhang, L. Gao, L. Wen, L. Heng and Y. Song, *Phys. Chem. Chem. Phys.*, 2013, **15**, 11943.
21 D. Wang, K. Zhou, M. Sun, Z. Fang, X. Liu and X. Sun, *Anal. Methods*, 2013, **5**, 6576.
22 N. Vasimalai and S. Abraham John, *J. Mater. Chem. A*, 2013, **1**, 4475.
23 Z. Lin, F. Luo, T. Dong, L. Zheng, Y. Wang, Y. Chi and G. Chen, *Analyst*, 2012, **137**, 2394.
24 A. Jaiswal, S. S. Ghsoh and A. Chattopadhyay, *Langmuir*, 2012, **28**, 15687.
25 H. Ahn, S. Y. Kim, O. Kim, I. Choi, C.-H. Lee, J. H. Shim and M. J. Park, *ACS Nano*, 2013, **7**, 6162.
26 W. Xiao, Y. Luo, X. Zhang and J. Huang, *RSC Adv.*, 2013, **3**, 5318.
27 X. Zhang and J. Huang, *Chem. Commun.*, 2010, **46**, 6042.
28 L. Su, T. Shu, Z. Wang, J. Cheng, F. Xue, C. Li and X. Zhang, *Biosens. Bioelectron.*, 2013, **44**, 16.
29 N. Liu, L. Li, G. Cao and R. Lee, *J. Mater. Chem.*, 2010, **20**, 9029.
30 L. Q. Xu, K.-G. Neoh, E.-T. Kang and G. D. Fu, *J. Mater. Chem. A*, 2013, **1**, 2526.
31 J. H. Wendorff, S. Agarwal and A. Greiner, *Electrospinning: Materials, Processing, and Applications*, Wiley-VCH Verlag GmbH & Co. KGaA, 2012.
32 S. Ramakrishna, K. Fujihara, W. Teo, T. Lim and Z. Ma, *An Introduction to Electrospinning and Nanofibers*, World Scientific Publishing Company, Singapore, 2005.
33 J. Xie, Y. Zheng and J. Y. Ying, *JACS*, 2009, **131**, 888.
34 A. C. Balazs, T. Emrick and T. P. Russell, *Science*, 2006, **314**, 1107.
35 X. Yu, D. Y. Lei, F. Amin, R. Hartmann, G. P. Acunac, A. Guerrero-Martínez, S. A. Maier, P. Tinnefeld, S. Carregal-Romero and W. J. Parak, *Nano Today*, 2013, **8**, 480.
36 R. Elghanian, J. J. Storhoff, R. C. Mucic, R. L. Letsinger and C. A. Mirkin, *Science*, 1997, **277**, 1078.
37 Y. Bao, H. Fong and C. Jiang, *J. Phys. Chem. C*, 2013, **117**, 21490.
38 P. Wang, L. Zhang, Y. Xia, L. Tong, X. Xu and Y. Ying, *Nano Lett.*, 2012, **12**, 3145.
39 H. Zhu, M. Du, M. Zou, C. Xu, N. Lia and Y. Fu, *J. Mater. Chem.*, 2012, **22**, 930.
40 C. H. Lee, L. Tian, A. Abbas, R. Kattumenu and S. Singamaneni, *Nanotechnology*, 2011, **22**, 27531.
41 Z. Wu and R. Jin, *Nano Lett.*, 2010, **10**, 2568.
42 S. Goel, K. A. Velizhanin, A. Piryatinski, S. A. Ivanov and S. Tretiak, *J. Phys. Chem. C*, 2012, **116**, 3242.
43 Xi. Wen, P. Yu, Y. R. Toh and J. Tang, *J. Phys. Chem. C*, 2012, **116**, 11830.
44 K. E. Roskov, K. A. Kozek, W.-C. Wu, R. K. Chhetri, A. L. Oldenburg, R. J. Spontak and J. B. Tracy, *Langmuir*, 2011, **27**, 13965.
45 C.-L. Zhang, K. P. Lv, H.-P. Cong and S.-H. Yu, *Small*, 2012, **8**, 648.
46 A. G. Destaye, C. K. Lin and C.-K. Lee, *ACS Appl. Mater. Interfaces*, 2013, **5**, 4745.
47 J. Wang, H.-B. Yao, D. He, C.-L. Zhang and S.-H. Yu, *ACS Appl. Mater. Interfaces*, 2012, **4**, 1963.
48 C. Tang, C. D. Saquing, J. R. Harding and S. A. Khan, *Macromolecules*, 2010, **43**, 630.
49 Y. Si, X. Wang, Y. Li, K. Chen, J. Wang, J. Yu, H. Wang and B. Ding, *J. Mater. Chem. A*, 2014, **2**, 645.
50 X. Wang, Y. Si, X. Mao, Y. Li, J. Yu, H. Wang and B. Ding, *Analyst*, 2013, **138**, 5129.
51 Y. Si, X. Wang, Y. Li, K. Chen, J. Wang, J. Yu, H. Wang and B. Ding, *J. Mater. Chem. A*, 2014, **2**, 645.
52 J. Xie, Y. Zheng and J. Y. Ying, *Chem. Commun.*, 2010, **46**, 961.
53 J.-S. Lee, M. S. Han and C. A. Mirkin, *Angew. Chem., Int. Ed.*, 2007, **46**, 4093.